Supercond. Sci. Technol. **22** (2009) 062001 (6pp) doi:10.1088/0953-2048/22/6/062001

RAPID COMMUNICATION

Dynamic magneto-optical imaging of transport current redistribution and normal zone propagation in $YBa_2Cu_3O_{7-\delta}$ coated conductor

Honghai Song[1,2], **Michael W Davidson**[3] **and Justin Schwartz**[1,4]

[1] Applied Superconductivity Center, National High Magnetic Field Laboratory, Florida State University, Tallahassee, FL 32310, USA
[2] Department of Electrical and Computer Engineering, FAMU-FSU College of Engineering, Florida State University, Tallahassee, FL 32310, USA
[3] Optical Microscopy division, National High Magnetic Field Laboratory, Florida State University, Tallahassee, FL 32310, USA
[4] Department of Mechanical Engineering, FAMU-FSU College of Engineering, Florida State University, Tallahassee, FL 32310, USA

Received 14 March 2009, in final form 6 May 2009
Published 19 May 2009
Online at stacks.iop.org/SUST/22/062001

Abstract

$YBa_2Cu_3O_{7-\delta}$ (YBCO) coated conductors carry high critical current density with the potential for low cost and thus have a broad range of potential applications. An unresolved issue that could inhibit implementation, however, is a lack of understanding of the current redistribution and normal zone propagation behavior in the event of a thermal disturbance (quench). In this work, we for the first time present the real-time, dynamic observation of magnetic field redistribution during a thermal disturbance via magneto-optical imaging with a high speed, high resolution CCD (charge coupled device) camera. The optical images are converted to a two-dimensional, time-dependent data set that is then analyzed quantitatively. It is found that the normal zone propagates non-uniformly in two dimensions within the YBCO layer. Two stages of normal zone propagation are observed. During the first stage, the normal zone propagates along the conductor length as the current and magnetic field redistribute within the YBCO layer. During the second stage, current sharing with the Cu begins and the magneto-optical image becomes constant. The normal zone propagation velocity at 45 K, $I = 50$ A ($\sim$50% I_c), is determined as 22.7 mm s^{-1} using the time-dependent optical light intensity data.

(Some figures in this article are in colour only in the electronic version)

1. Introduction

$YBa_2Cu_3O_{7-\delta}$ (YBCO) coated conductors (CC) with very high critical current density (J_c) over a broad range of magnetic field and temperature are now commercially available [1, 2]. One of the remaining critical issues to be addressed for these conductors to be effectively applied to functional power applications is to understand quench-related behaviors, including current redistribution within the complex conductor architecture and effective means of quench detection [3, 4]. A number of groups have shown that high temperature superconductors (HTS) are significantly more stable than NbTi and Nb_3Sn magnets with as much as two orders-of-magnitude higher minimum quench energy (MQE) [5–14]. With high quench energy also comes a very slow normal zone propagation velocity (NZPV), and of the HTS conductors, YBCO CCs are the most stable but also have the slowest NZPV. Despite extensive study of the macroscopic quench behaviors

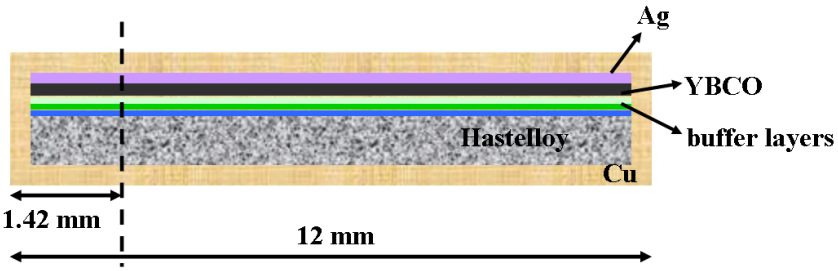

Figure 1. Illustration of the transverse cross-section of a 12 mm wide a YBCO CC, showing architecture (top to bottom) of 20–25 μm Cu, 2 μm Ag, 1–3 μm YBCO, 1 μm buffer layers, 50 μm Hastelloy and 20 μm Cu. Also illustrated is the 1.42 mm piece cut from the edge for MOI investigation.

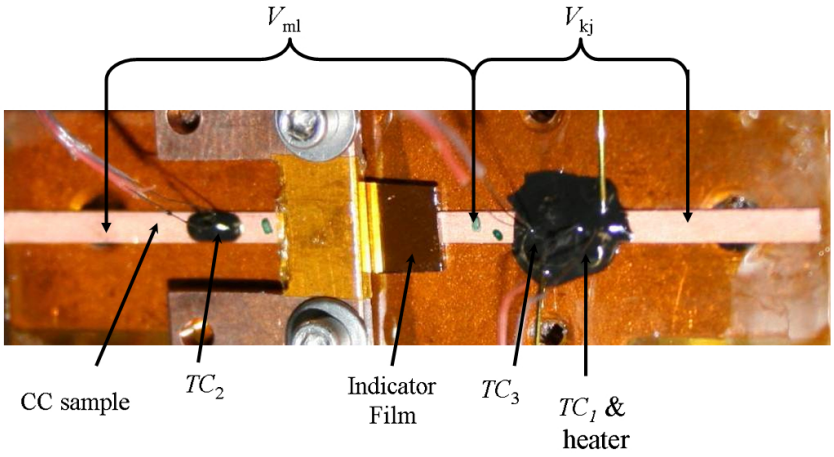

Figure 2. A photo of the mounted and instrumented sample on the MOI cold finger.

(MQE, NZPV), there is little understanding of the dynamic, microscopic behavior during the development of a normal zone and quench. The microscopic behavior, however, dictates the time-dependent, highly localized temperature and temperature gradients which in turn dictate if the conductor is damaged. Thus, the development of effective approaches to quench detection and protection require a more detailed understanding of the microscopic behaviors. Recently, visualization of normal zone propagation in YBCO CC has been demonstrated through fluorescent paints [15] and a digital speckle pattern interferometer [16]. Neither of these approaches, however, provides sufficiently detailed information regarding the current distribution as a function of time and space.

Magneto-optical imaging (MOI) is a technique that facilitates the real-time visualization of two-dimensional magnetic field distributions using Faraday rotation through a magneto-optically active indicator film. This technique has been extensively developed for studying static or slowly varying magnetic field distributions in superconductors, revealing inhomogeneities due to original defects, low angle grain boundaries, external strain, ac behavior, etc [17–29]. Here we report on the application of MOI to the dynamic problem of current redistribution during the initiation and propagation of a heater-induced normal zone. In this experiment, the detecting MO indicator is sensitive to the perpendicular component of magnetic field. Here, this magnetic field is the self-field generated by a transport current in the YBCO sample. Self-field calculations using the critical state model [30] finds that the perpendicular component is variable across the sample width.

2. Experimental approach

The MOI system reported previously [17, 31] is enhanced with a high speed, high resolution digital camera (Hamamatsu EM-CCD C9100). The maximum observation area is 1.58 × 1.58 mm^2, which corresponds to 512 pixels × 512 pixels. With this system, the optimum exposure time per image is 68 ms, so the maximum NZPV that can be detected is 23.2 mm s^{-1}. Referring to previous results [12], we operate at an initial temperature $T_0 = 45$ K and $I/I_c \sim 50\%$ where the NPZV $\sim$20 mm s^{-1} is expected and I is sufficiently large to provide an observable self-field on the order of tens of mT.

The essentials of the MOI setup, which are described at length elsewhere [17], include the sample mounted atop a rectangle cold finger within a vacuum cryostat cooled by flowing helium (14–77 K). The 40 mm long CC sample is 1.42 mm wide, having been cut from an original 12 mm wide, high J_c sample provided by Superpower, Inc. as illustrated in figure 1. The conductor is described in detail elsewhere [32]. It is necessary to reduce the sample width in order to reduce I_c; otherwise the heat load through the current leads is too large and an inhomogeneous, time-dependent temperature distribution results. As illustrated in figure 1, for this

experiment the sample is cut from the edge of the conductor and includes the Cu stabilizer that links the Ag cap layer to the underlying Hastelloy substrate. The sample is attached tightly to a Kapton tape which is glued to the upper surface of the cold finger. A nichrome (80%Ni, 20%Cr) wire heater (0.203 mm diameter) and three type-E thermocouples (TC) are tightly mounted to the upper surface of the sample using Stycast 2850FT. The iron garnet indicator film (Bi:YIG) is mounted atop the sample with a copper clamp to reduce the gap between the sample surface and indicator film. The separation between the bottom of the indicator film and the upper surface of the sample is less than 10 μm. TC_1 is in the center of the heater, TC_2 is on the far end of the sample on the other side of indicator film as the heater, and TC_3 is between the heater and the indicator film. Lastly, two pairs of voltage taps are mounted to the sample surface using silver paint. V_{kj} is across the heater section and V_{ml} encompasses the section that includes the indicator film and TC_2. A photo of the mounted and instrumented sample is seen in figure 2. The transport current is fed from the ends of the sample (not seen in figure 2).

The MOI system is not designed for high current *in situ* I_c measurements as there are limits to the amount of current that can be transported by the current leads and to the thermal stability of the system due to heating of the leads. A 50 K *in situ* measurement showed $I_c(50\ \mathrm{K}) = 87.9$ A, but it was considered too risky to test at higher current. Thus, the $I_c(45\ \mathrm{K})$ of the cut sample is estimated. The original 12 mm wide sample has $I_c(77\ \mathrm{K}) = 320$ A, as measured by SuperPower Inc. Assuming that it is homogeneous across the width, and factoring out the 25 μm of Cu on the edges, the 1.42 mm wide cut sample has $I_c(77\ \mathrm{K}) = 37.4$ A. Using the $I_c(50\ \mathrm{K})$ and $I_c(77\ \mathrm{K})$ values, $I_c(45\ \mathrm{K}) = 97.3$ A by linear extrapolation. Thus, $I = 50$ A is roughly 50% of $I_c(45\ \mathrm{K})$.

The transport current is provided by a Hewlett Packard power supply in a constant-current state. This power supply has been used in many previous quench studies and is sufficiently stable that the current does not vary as the sample resistance increases with increasing temperature. To study the quench behavior within the MOI system, I is ramped quickly to 50 A and held for 200 ms to reach equilibrium. The heater is then pulsed for nominally 600 ms (the Keithley DMM response time is 10–25 ms) to induce a normal zone. If the heat pulse does not induce a quench, then the procedure is repeated with increased heat pulse amplitude until a quench occurs. In this experiment a quench occurred for a pulse voltage of 7.5 V which, for a 600 ms heat pulse, corresponds to ~3.2 J.

3. Experimental results

The MOI's CCD camera is synchronized to capture a sequence of images at 68 ms intervals before and during quenching. After the transport current is established, the $t = 0$ image, shown in figure 3(a), is obtained. The MO light intensity is proportional to the perpendicular component of the magnetic field. Figure 3(b) plots light intensity profiles across the width at $X = 210$ at both 0 ms (current flowing in YBCO layer before the heater pulse) and 545 ms (current flowing in the Cu stabilizer). Since the current penetrates symmetrically from

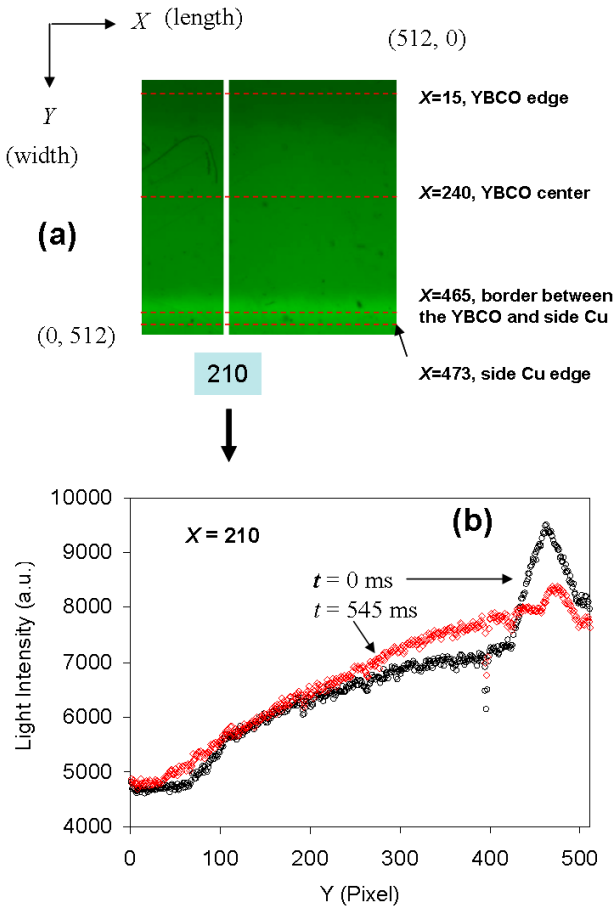

Figure 3. (a) The MOI image illustrates the magnetic field profile of the full YBCO width after the transport current is established and before the heater is pulsed. The observation area is 512 × 512 in an XY coordinate system. (b) Light intensity plots along the width at $X = 210$, $t = 0$ ms, with transport current in the YBCO layer before the heater is pulsed, and $t = 545$ ms when the current is shared in the surrounding Cu stabilizer.

the edges nominally and the self-field is expected to be anti-symmetric according to the Critical State Model [30], the light intensity has two peaks. The slight asymmetry between the peaks is likely caused by either uneven separation between the bottom of the indicator film and the upper surface of the sample, or inhomogeneous superconducting properties across the sample width.

The graph in figure 4 plots V_{ml}, V_{kj}, TC_1, TC_2 and TC_3 as a function of time, where the time-axis is adjusted such that $t = 0$ is defined as the beginning of the pulse. Similar to what has been seen previously [5, 11, 12], TC_1 and TC_3 increase rapidly almost immediately due to proximity to the heater, whereas TC_2 shows a considerable time delay. When a measurable, non-zero V_{kj} appears at $t = 78$ ms, $TC_1 = 94$ K and $TC_3 = 62$ K. Measurable V_{ml} appears at $t = 169$ ms when the normal zone propagation reaches that section. After the pulse ends at $t = 619$ ms, TC_1 and TC_3 decrease slightly, as does the slope of $V_{kj}(t)$, while TC_2 and V_{ml} continue to increase due to joule heating and heat conduction.

MOI images are captured after the heater pulse begins at $t = 0$ ms, with the first image captured at $t = 1$ ms.

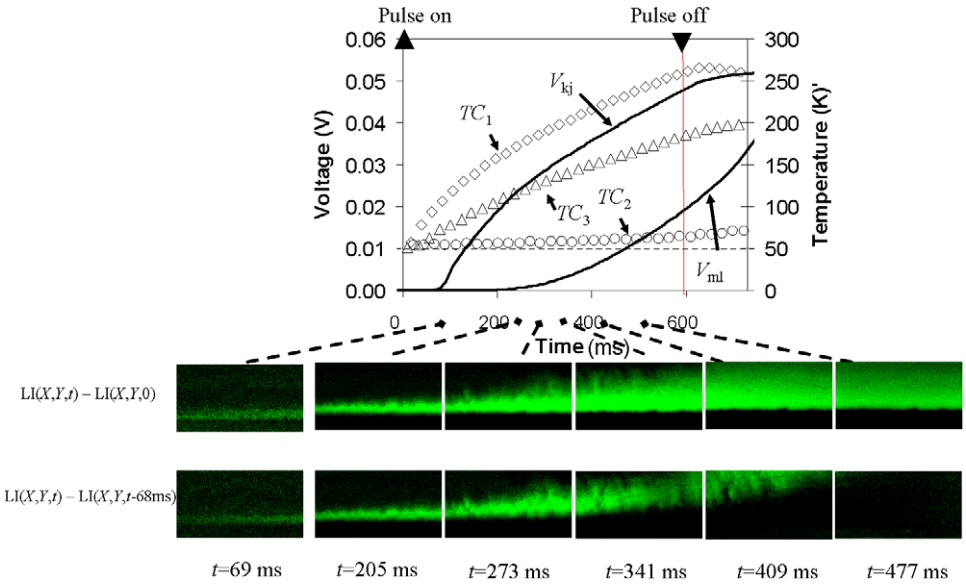

Figure 4. The graph plots the time-dependent voltages and temperatures during a quench with $I = 50$ A and $V_P = 7.5$ V at 45 K. $t = 0$ is defined as the beginning of the heater pulse; the current is established prior to that. The sequence of MOI images, whose time-stamps are illustrated relative to the graph, are results from the two differentiation methods that show the dynamic penetration of magnetic field into the CC due to normal zone propagation.

The differentiated image has almost one-half of the vertical width of the original (full) image while keeping the horizontal length constant. As the sensitivity of the camera is greater than that of the human eye, the images are treated as a data set of light intensity as a function of location and time, $LI(X, Y, t)$, where the X and Y directions are illustrated in figure 3 and are in one pixel increments numbered from zero to 512. The temporal data are obtained in 68 ms intervals. Changes in the magnetic field profile are more effectively seen via two image differentiation methods. In the first, $LI(X, Y, t)$–$LI(X, Y, 0)$ is viewed; this is shown in the first row of images below the graph in figure 4. Here only the lower half of the images (pixels $240 < Y < 512$) are shown since $X = 240$ is the centerline of the YBCO layer.; In the second approach, $LI(X, Y, t)$–$LI(X, Y, t\text{-}68$ ms) is plotted, thereby illustrating the change in profile during the most recent time period. These are seen in the lower row of images in figure 4.

Observable changes in the images begin at $t = 69$ ms, which is after the initial increases in TC_1 and TC_3 but slightly before V_{kj} becomes measurably non-zero at $t = 78$ ms, indicating that the MOI is more sensitive than the voltage measurement. The sequence of images seen in figure 4 captures the magnetic field penetration from the sample edge (bottom of the image) to the sample center line. During this magnetic field (and current) redistribution process, the local temperature increases but remains below the current sharing temperature; i.e., $T_0 < T < T_{cs}$, where $T_{cs} \sim 71$ K is interpolated from the I_c data at 77 and 50 K. Note that T_{cs} is the temperature at which the I_c of the bridge decreases to the transport current (50 A) The normal zone 'wavefront' is diagonally shaped, revealing that normal zone propagation is non-uniform in the X-direction. Due to the symmetry of current distribution across the entire width ($0 < Y < 512$), although figure 4 shows only the half-width ($240 < Y < 512$), the full-width would show two diagonals forming a '>-shape'. Full penetration is seen in at $t = 481$ ms. We refer to the time for which $T_0 < T < T_{cs}$, which ends when the images become constant, as current redistribution. Any subsequent temperature increase lowers the local I_c below I, causing current sharing with the Cu stabilizer. Note that since the Cu is not only above the YBCO layer but also adjacent to it (at the bottom of the MOI images; see figure 1), the transition into the current sharing regime includes a small shift in the width of the current carrying area, which is seen subtly as an upward shift in the black/green boundary at the bottom of the differentiation images ($LI(X, Y, t)$–$LI(X, Y, 0)$).

To further the quantitative analysis and distinguish current redistribution from current sharing, figure 5 plots $LI(X = 10, Y)$ and $LI(X = 510, Y)$ with each curve representing a different time interval between $t = 1$ and 749 ms. Note that this is the light intensity data, not the differentiated data. The data from only the bottom portion of the images are plotted, $420 < Y < 512$. For $X = 10$, which is further from the heater, the peak in LI decreases from $t = 1$ to 409 ms. Subsequently, beginning at $t = 477$ ms, $LI(Y)$ becomes time invariant. Note the rapid shift in the location of the $LI(Y)$ peak from $Y = 463$ at $t = 409$ ms to $Y = 471$ at $t = 545$ ms. This represents the transition from current redistribution within the YBCO to current sharing with the Cu. The $t = 409$ ms curve also illustrates the non-uniformity of the normal zone propagation; for lower values of Y, this curve follows that of the early curves, whereas at the other end of the plot (higher Y values, corresponding to the bottom of the images), the curve is overlapping with the higher t data. The data for $X = 510$ show the same behavior, but the shift occurs from $t = 341$ to 409 ms because this section is closer to the heater. In general, the current redistribution at $X = 510$ is about one time-step ahead that at $X = 10$, indicating that the propagation time is

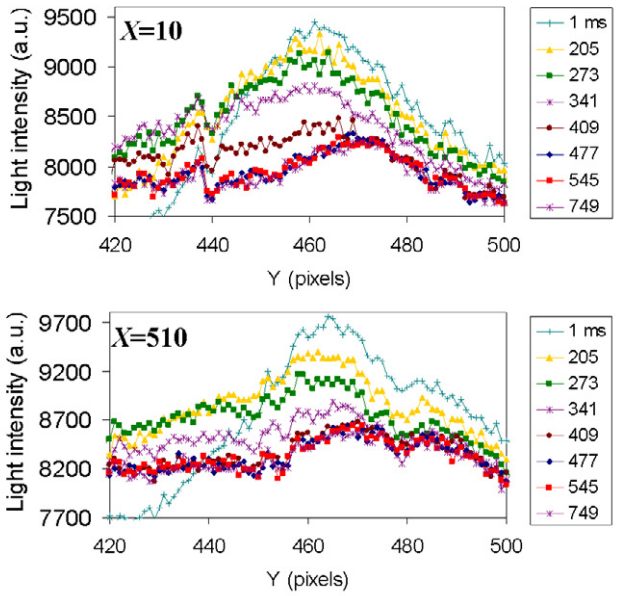

Figure 5. Light intensity as a function of location across the width of the CC at two locations along the length. Each curve is a different time-stamp in ms. These graphs illustrate the non-uniform transition from current redistribution to current sharing.

about one time-step. Note that, since the observation width of 1.58 mm contains 512 pixels, and the width of the side Cu is ∼25 μm, the YBCO center across the width is at $X = 240$, rather than the geometrical center $X = 256$ as illustrated in figure 3.

Normal zone propagation is evaluated in more detail in figure 6, which plots $LI(X, Y, t)$–$LI(X, Y, 0)$ for $X = 10$ and 510 and four different time-steps. Note that it shows light intensity differentiation over the entire width rather than the half-width shown in figure 4. In each case, the data for $X = 510$ are nominally one time-step earlier than for $X = 10$. At the first three time-steps, the data overlap for most Y-values but with a small gap which narrows as time progresses, until in the last graph, which corresponds to the current sharing stage, the data overlap for all Y. This indicates that, while the normal zone propagation time from $X = 510$ to 10 is about one time-step (68 ms), it is non-uniform across the width of the cross-section. Considering that 512 pixels correspond to 1.58 mm, the distance from $X = 510$ and 10 is 1.54 mm, the nominal NZPV is 22.7 mm s^{-1}. At the microscopic level, however, the NZPV is spatially varying, so this value is only a nominal average. Also note that the NZPV depends on temperature and current; this value is for 45 K, $I = 50$ A (∼50%I_c).

In summary, we dynamically visualize normal zone propagation in YBCO CC using MOI and find that the current and magnetic field redistribution proceeds non-uniformly in two directions. The normal zone propagation front is diagonally shaped while moving along the conductor length. The real-time images are converted to a two-dimensional time-varying data set, providing additional insight into the current and magnetic field redistribution process and also establishing a new application of magneto-optical imaging. Using this approach, the NZPV at 45 K is calculated as 22.7 mm s^{-1} for $I = 50$ A (∼50% I_c).

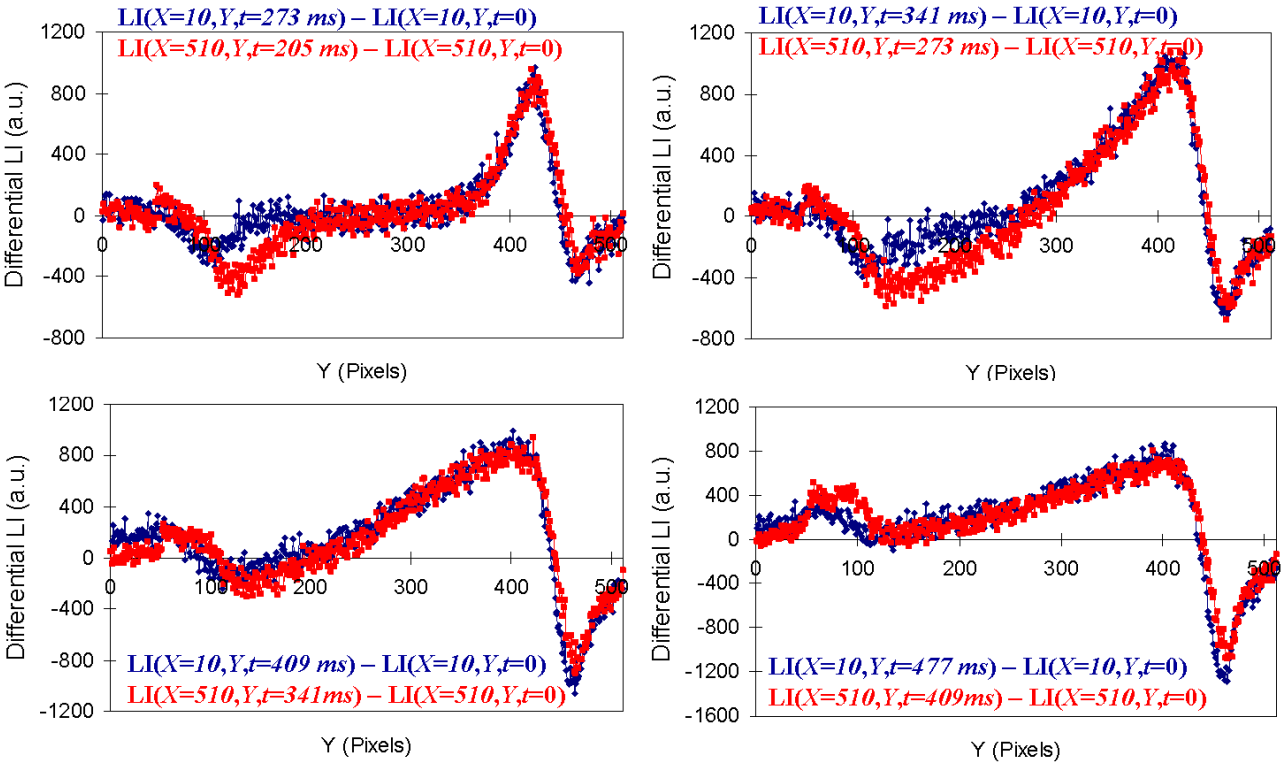

Figure 6. Differential light intensities at $X = 10$ and 510 at four different times. The times for $X = 10$ is one step later than that of $X = 510$ in each image.

Acknowledgments

The authors thank Y Y Xie and his colleagues at SuperPower, Inc., for providing the high quality YBCO CC sample used in this study. This work supported in part by the Air Force Research Laboratory.

References

[1] Malozemoff A P *et al* 2008 *Progress in High Temperature Superconductor Coated Conductors and Their Applications* (Bristol: Institute of Physics Publishing)

[2] Selvamanickam V, Chen Y, Xiong X, Xie Y, Zhang X, Rar A, Martchevskii M, Schmidt R, Lenseth K and Herrin J 2008 Progress in second-generation HTS wire development and manufacturing *Physica* C **468** 1504–9

[3] Larbalestier D, Gurevich A, Feldmann D M and Polyanskii A 2001 High-T_c superconducting materials for electric power applications *Nature* **414** 368–77

[4] Schwartz J *et al* 2008 High field superconducting solenoids via high temperature superconductors *IEEE Trans. Appl. Supercond.* **18** 70–81

[5] Wang X R, Caruso A R, Breschi M, Zhang G M, Trociewitz U P, Weijers H W and Schwartz J 2005 Normal zone initiation and propagation in Y–Ba–Cu–O coated conductors with Cu stabilizer *IEEE Trans. Appl. Supercond.* **15** 2586–9

[6] Duckworth R C, Lue J W, Lee D E, Grabovickic R and Gouge M J 2003 The role of nickel substrates in the quench dynamics of silver coated YBCO tapes *IEEE Trans. Appl. Supercond.* **13** 1768–71

[7] Ishiyama A, Yanai M, Morisaki T, Ueda H, Shiohara Y, Izumi T, Iijima Y and Saitoh T 2005 Normal transition and propagation characteristics of YBCO tape *IEEE Trans. Appl. Supercond.* **15** 1659–62

[8] Trillaud F, Ahn M C, Bascunan J, Kim W S, Voccio J P and Iwasa Y 2008 Quench behavior, quench protection of a YBCO test coil assembly *IEEE Trans. Appl. Supercond.* **18** 1329–32

[9] Kim W S, Trillaud F, Ang I C, Hahn S Y and Iwasa Y 2007 Normal zone propagation in YBCO winding pack models *IEEE Trans. Appl. Supercond.* **17** 2478–81

[10] Grabovickic R, Lue J W, Gouge M J, Demko J A and Duckworth R C 2003 Measurements of temperature dependence of the stability and quench propagation of a 20 cm-long RABiTS Y–Ba–Cu–O tape *IEEE Trans. Appl. Supercond.* **13** 1726–30

[11] Trillaud F, Palanki H, Trociewitz U P, Thompson S H, Weijers H W and Schwartz J 2003 Normal zone propagation experiments on HTS composite conductors *Cryogenics* **43** 271–9

[12] Wang X, Trociewitz U P and Schwartz J 2007 Near-adiabatic quench experiments on short $YBa_2Cu_3O_{7-\delta}$ coated conductors *J. Appl. Phys.* **101** 053904

[13] Sokolovsky V and Meerovich V 2008 Normal zone propagation along superconducting films deposited on wide substrates *Cryogenics* **48** 397–405

[14] Levin G A and Barnes P N 2007 The normal zone in $YBa_2Cu_3O_6 + x$-coated conductors *Supercond. Sci. Technol.* **20** 1101–7

[15] Ishiyama A, Tsuchiya M, Ueda H and Shiohara Y 2007 Assessment of cryogenic thermography system using commercial fluorescent paints on their applicability to visualization of normal-zone propagation in YBCO coated conductor *IEEE Trans. Appl. Supercond.* **17** 3765–8

[16] Angurel L A, Martinez E, Lera F, Recuero S, Andres N, Arroyo M P, Xie Y Y and Selvamanickam V 2008 Quench detection in $YBa_2Cu_3O_{7-\delta}$ coated conductors using interferometric techniques *J. Appl. Phys.* **104** 093916

[17] van der Laan D C, Davidson M W, ten Haken B, ten Kate H H J and Schwartz J 2002 Magneto-optical imaging study of the crack formation in superconducting tapes caused by applied strain *Physica* C **372–376** 1020–3

[18] Feldmann D M *et al* 2001 Magneto-optical imaging of transport currents in $YBa_2Cu_3O_{7-x}$ on RABiTS (TM) *IEEE Trans. Appl. Supercond.* **11** 3772–5

[19] Bobyl A V, Shantsev D V, Galperin Y M, Johansen T H, Baziljevich M and Karmanenko S F 2002 Relaxation of transport current distribution in a YBaCuO strip studied by magneto-optical imaging *Supercond. Sci. Technol.* **15** 82–9

[20] Dorosinskii L A, Indenbom M V, Nikitenko V I, Ossipyan Y A, Polyanskii A A and Vlaskovlasov V K 1992 Studies of HTSC crystal magnetization features using indicator magnetooptic films with inplane anisotropy *Physica* C **203** 149–56

[21] Villaume A, Antonevici A, Bourgault D, Leggeri J P, Porcar L and Villard C 2008 Magneto-optical setup for *in situ* strain and transport measurements on superconductors *Rev. Sci. Instrum.* **79** 023904

[22] Rutel I B, McIntosh C, Caruso A, Davidson M W and Schwartz J 2004 Quantitative analysis of current density distributions from magneto-optical images of superconducting $YBa_2Cu_3O_{7-\delta}$ thin films *Supercond. Sci. Technol.* **17** S269–73

[23] Jooss C, Albrecht J, Kuhn H, Leonhardt S and Kronmuller H 2002 Magneto-optical studies of current distributions in high-T_c superconductors *Rep. Prog. Phys.* **65** 651–788

[24] Lucarelli A, Lupke G, Haugan T J, Levin G A and Barnes P N 2006 Time-resolved magneto-optical imaging of $Y_1Ba_2Cu_3O_{7-\delta}$ thin films in high-frequency AC current regime *Supercond. Sci. Technol.* **19** 667–70

[25] Goa P E, Hauglin H, Baziljevich M, Il'yashenko E, Gammel P L and Johansen T H 2001 Real-time magneto-optical imaging of vortices in superconducting $NbSe_2$ *Supercond. Sci. Technol.* **14** 729–31

[26] Polyanskii A A, Gurevich A, Pashitski A E, Heinig N F, Redwing R D, Nordman J E and Larbalestier D C 1996 Magneto-optical study of flux penetration and critical current densities in [001] tilt $YBa_2Cu_3O_{7-\delta}$ thin-film bicrystals *Phys. Rev.* B **53** 8687–97

[27] Vanderbemden P, Hong Z, Coombs T A, Denis S, Ausloos M, Schwartz J, Rutel I B, Babu N H, Cardwell D A and Campbell A M 2007 Behavior of bulk high-temperature superconductors of finite thickness subjected to crossed magnetic fields: experiment and model *Phys. Rev.* B **75** 174515

[28] Albrecht J, Djupmyr M and Bruck S 2007 Universal temperature scaling of flux line pinning in high-temperature superconducting thin films *J. Phys.: Condens. Matter* **19** 216211

[29] Johansen T H, Baziljevich M, Bratsberg H, Galperin Y, Lindelof P E, Shen Y and Vase P 1996 Direct observation of the current distribution in thin superconducting strips using magneto-optic imaging *Phys. Rev.* B **54** 16264–9

[30] Bean C P 1964 Magnetization of high-field superconductors *Rev. Mod. Phys.* **36** 31

[31] van der Laan D C, van Eck H J N, ten Haken B, ten Kate H H J and Schwartz J 2003 Strain effects in high temperature superconductors investigated with magneto-optical imaging *IEEE Trans. Appl. Supercond.* **13** 3534–9

[32] Selvamanickam V *et al* 2009 High performance 2G wires: from R&D to pilotscale manufacturing *IEEE Trans. Appl. Supercond.* **19** at press